Atmospheric Research 295 (2023) 106964

Contents lists available at ScienceDirect

Atmospheric Research

journal homepage: www.elsevier.com/locate/atmosres

Cascade sensitivity tests to model deep convective systems in complex orography with WRF

Francesco Ferrari [a,*], Enrico Maggioni [b], Alessandro Perotto [b], Raffaele Salerno [c], Mauro Giudici [a]

[a] Università degli Studi di Milano, Department of Earth Sciences, Italy
[b] Ideam srl, Cinisello Balsamo (MI), Italy
[c] Meteo Expert, Cinisello Balsamo (MI), Italy

ARTICLE INFO

Keywords:
Deep convective events
WRF cascade sensitivity test
Cloud microphysics
Planetary boundary Layer
Surface layer
Land-Surface model

ABSTRACT

The goal of the present study is to improve the analysis of the performance of the Weather Research and Forecasting (WRF) model, Version 4.3.3, under different settings, in the prediction of precipitation in case of deep convective events. This is done through a wide cascade sensitivity test involving parameterizations expected to play a major role in the description of precipitation for deep convective events: cloud microphysics (CM), planetary boundary layer (PBL), surface layer (SL) and land-surface (L-S) model. Four significant precipitation events, which were associated to deep convective systems and occurred between 2019 and 2021 in Lombardia and Liguria regions (Northern Italy), have been simulated according to 45 different WRF settings. High resolution simulations are required when dealing with small scale deep convective systems as well as a suitable verification method. So, traditional statistical indexes have been integrated with new-generation verification methods, based on the identification of precipitation patterns in forecast and observed fields and on the evaluation of their similarity through the calculation of a coupling index. This analysis method has been exploited to evaluate the quality of the high-resolution simulations performed, and to individuate the best-performing WRF setting in simulating intense convective events. From the present work emerges how the unique CM parameterization characterized by a triple-moment treatment for cloud ice significantly outperforms all other CM schemes underlying the main role of cloud ice in the description of the precipitation case studies. Furthermore, PBL and L-S schemes show a leading role, at least as much as CM, in the description of the events.

1. Introduction

The simulation of extreme precipitation events is a major challenge for numerical weather models. North-West Italy is a natural laboratory where the performances of numerical models can be tested. Here, in fact, the interaction between a very steep and complex orography, provided by Alps and Apennines ranges, and a deep sea, as in the case of the Ligurian Sea, supply natural ingredients for the development of extreme events. Favourable conditions develop all year round, but are particularly frequent during Summer and Fall. Modeling situations in which convection dominates is very challenging; an accurate description and simulation of the mechanisms and processes that rule the triggering, the localization and the evolution of these precipitation systems is extremely tricky. The complex multi-scale interaction among moist ambient inflow, sea and orography makes difficult the precise prediction of location, timing and amount of precipitation associated with these systems (Miglietta and Davolio, 2022). Furthermore, the high population density in these areas prompts the need for the development of a reliable weather prediction system.

Motivated by these objectives, the goal of the present study is to perform a wide sensitivity test of different parameterization schemes available in the Weather Research and Forecasting (WRF) model, Version 4.3.3 (Skamarock et al., 2008), and to define an objective analysis method able to emphasize also small differences present in the analyzed simulations.

Parameterizations are responsible for the description of sub-grid scale phenomena and persist as one of the most challenging problems in numerical modeling of the atmosphere (Pielke, 2013). A huge variety of parameterizations have been developed during the years to describe main unresolved phenomena, but, due to their semi-empirical nature, it is important to perform intercomparison and sensitivity studies to understand which scheme can be appropriately used for individual cases.

* Corresponding author.
E-mail address: francesco.ferrari2@unimi.it (F. Ferrari).

https://doi.org/10.1016/j.atmosres.2023.106964
Received 10 March 2023; Received in revised form 10 August 2023; Accepted 12 August 2023
Available online 29 August 2023

Parameterization schemes involved in the present study concern cloud microphysics (CM), planetary boundary layer (PBL), surface layer (SL) and land-surface (L-S) models. All these parameterizations are expected to play a major role in the description of precipitation in case of deep convective events. CM schemes compute the evolution of atmospheric hydrometeors as water vapor, cloud liquid water, cloud ice and other types of precipitation, being therefore crucial for a correct prediction of heavy rainfall events. In fact, microphysical processes directly impact buoyancy, and hence convective fluxes, and have been the object of many works concerning both real (Rajeevan et al., 2010; Douluri and Chakraborty, 2021) and idealized cases (Morrison and Milbrandt, 2011; Bryan and Morrison, 2012). PBL and SL schemes, describing transport of moisture, heat and momentum from ground surface to higher atmospheric levels, are fundamental in simulating stability of the lower atmosphere, eventually triggering convection, vertical mixing and availability of moisture (Coniglio et al., 2013; Shin and Hong, 2011). The vertical eddy transport in the PBL determines the vertical profiles of low-level moisture, temperature and winds (Roebber et al., 2004), and rules the thermodynamic instability, impacting on convection and precipitation development (Hu et al., 2010; Holtslag et al., 2013; Clark et al., 2015; Cohen et al., 2015). In the WRF model, PBL parameterizations are categorized according to non-local or local turbulence closure assumptions (Wang et al., 2021). Parameterizations belonging to the first group determine the non-local sub-grid scale transport through a mass-flux term (Pleim, 2007; Pleim, 2007) or a gradient-adjustment gamma term (Hong et al., 2006); they are typically characterized by overly vigorous vertical mixing, which favours the simulation of deep, dry and warm boundary layers (Burlingame et al., 2017). The second group generally adopts turbulent kinetic energy (TKE) closure schemes and only adjacent vertical levels are taken into account to evaluate the turbulent fluxes. In this case, the simulated vertical mixing is relatively weak and more likely produces shallow, cool and moist boundary layers (Burlingame et al., 2017). Many studies have analized model sensitivity in regard to the PBL scheme chosen, mainly exploring heavy precipitation related to tropical cyclones (Braun and Tao, 2000; Li and Pu, 2008; Liu et al., 2017; Dong et al., 2019). Some works, however, examined also the PBL effect on severe convective events at midlatitudes (Efstathiou et al., 2013; Srinivas et al., 2018) and produced somehow contrasting results regarding performances of local and non-local closure schemes, highlighting the necessity of further investigation. Finally, the S-L models have been identified to play a key role in the simulation of extreme events, since they are responsible for energy and water exchanges at the ground surface (Lorenz et al., 2016). It has been shown that the increase in extreme precipitation can be related to land surface heterogeneities and urbanization processes (Han and Baik, 2008; Niyogi et al., 2011), especially when these extreme rainfall events occur under weak synoptic forcing (Chen et al., 2014; Xu et al., 2012). In particular, the impact of small-scale land surface heterogeneities can affect both convective initiation and convective development when convective-permitting models are exploited (Gao et al., 2021).

Proper description of events related to deep convective systems requires to explicitly resolve convection. High resolution simulations are thus required (Lack et al., 2010; Gilleland et al., 2009; Cassola et al., 2015), introducing the problem of exploiting a reliable verification method to evaluate performances of the model. In fact, when the model resolution is increased up to a few kilometres, traditional point-wise verification methods become critical, due to the 'double penalty' error (Casati et al., 2008), that results in a fictitious penalty of high-resolution simulations in comparison to coarser simulations. To overcome this problem, new-generation spatial verification methods, based on the identification of patterns (i.e. areas above a certain precipitation threshold) in forecast and observed fields and the evaluation of their similarity through the calculation of a coupling index (*CI*), have been developed (Davis et al., 2006; Davis et al., 2006).

This paper is intended as a basic step in which the identified best performing WRF setting together with the defined analysis method will provide the instruments for future evaluation of the impact on WRF simulations of different data assimilation methods. Case studies are briefly introduced in Section 2, while WRF setup is presented in Section 3. The analysis methodology and the results of the cascade sensitivity test are reported in Sections 4 and 5 respectively. Finally, conclusions are drawn up in Section 6.

2. Case studies and motivations

The case studies analyzed in the present paper are four severe convective events that affected the North-Western part of Italy, in particular the regions of Liguria and Lombardia, between 2019 and 2021, and that have been poorly predicted in operational forecasts. Two of the four cases, the first occurring on July 11 2020 and the second on September 16 2021, regard storms sparked by diurnal convective activity that characterizes foothill Alpine areas and adjacent plains during summer time. In both cases, geopotential height drops on the Alps due to a trough from central Europe (Fig. 1, panels *b*) and *c*)) triggering convective phenomena. In July 11 2020 a convective system developed in the early afternoon in the North-Western part of Lombardy. This system rapidly moved eastwards, finally affecting the eastern part of the region in the late afternoon. The amount of precipitation reached 30 mm in about 2 h (Maggioni et al., 2023). Fig. 2, panel *c*), shows 12-h accumulated precipitation (between 12 UTC of 11 July and 00 UTC of 12 July 2020) during the event.

September 16 2021 event is similar, and, again, it is associated to diurnal convection typical of sub-alpine and Apennine areas during summer time. In this case precipitation peaks reached almost 70 mm over short times (about 4 h), but precipitation resulted more widespread across Northern Italy with respect to the previous case (Fig. 2, panel *d*)). The other two events instead concern two floods that affected Liguria in October 21 2019 and October 4 2021. These flooding events were associated to quasi-stationary mesoscale deep convective systems, responsible for the majority of extreme precipitation events that quite often affect the central Mediterranean basin, and in particular Liguria, during Autumn (Buzzi et al., 2014; Rebora et al., 2013; Fiori et al., 2014; Cassola et al., 2016). The typical onset of these events is represented by a deep trough just west of Italy facing a blocking high pressure system affecting Eastern Europe and preventing the natural eastward movement of the trough (Fig. 1, panels *a* and *d*)). During these events, very intense precipitation was triggered by a convergence between two flows with different directions: a southerly, warm and moist flow over Tyrrhenian Sea and a northerly, cool and dry one, affecting the central part of the region. Furthermore, in the considered cases, the interaction between the above mentioned flows and the very steep orography that characterizes the central-western part of the Liguria, where mountains rise to about 1300 m in a very short distance from the sea, contributed to further enhance the intensity of the phenomena with the well known stau effect. Unlike the first two presented cases, Liguria events lasted for about 20 h, accumulating a huge amount of precipitation over very limited areas, as clearly visible from Fig. 2, panels *a*), *b*), *e*) and *f*), and resulting into two devastating floods. Especially during October 4 2021 event, precipitation intensity reached values that are very uncommon for mid-latitude areas, such as: 178 mm/hr and 378 mm/3 h at Urbe-Vara Superiore and 741 mm/12 h and 884 mm/ 24 h at Rossiglione, both villages located in the Liguria inland.

3. Model setup and sensitivity tests

For the present study, the WRF model, Version 4.3.3 was employed. The WRF model is a non–hydrostatic, fully compressible, primitive-equations model, and is thoroughly described in Skamarock et al. (2008). Simulations have been performed over a domain covering the North-Western part of Italy and characterized by a grid step of 1 km (Fig. 3, panel *b*)), allowing to explicitly solve convection. A convection-permitting resolution is fundamental when dealing with deep convective

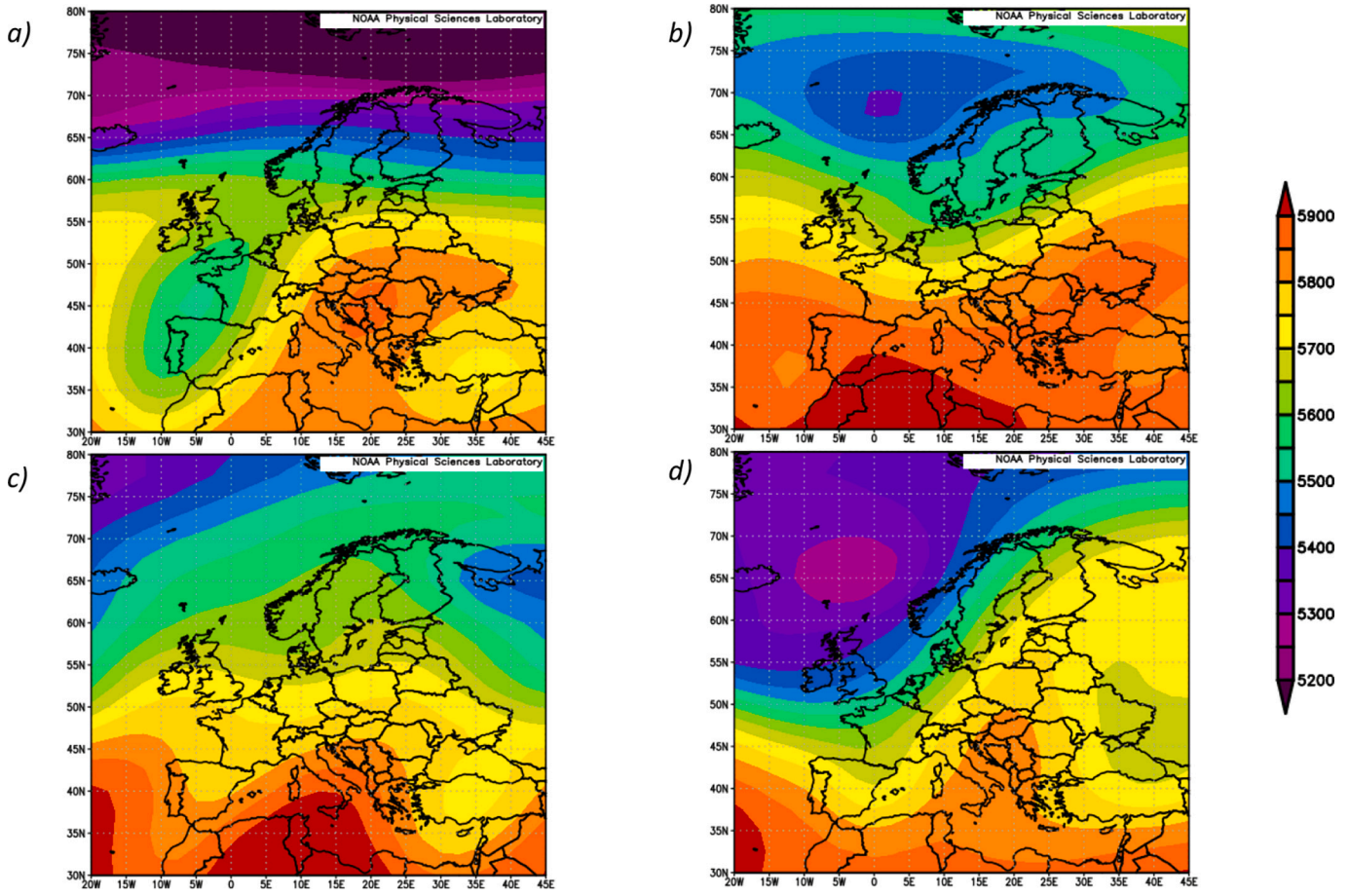

Fig. 1. Reanalysis of 500-mb geopotential height [m] for October 21 2019, panel *a*), July 11 202, panel *b*), September 16 2021, panel *c*) and October 4 2021, panel *d*). Source *https : //psl.noaa.gov/data/composites/day/*.

systems (Cassola et al., 2015; Gilleland et al., 2009; Ferrari et al., 2021); the domain has been nested with a two-way coupling in a parent domain covering the Central and Northern part of Italy and the Alpine region (Fig. 3, panel *a*)) with a grid step of 4 km. For all simulations performed, the number of terrain-following vertical levels adopted was 37 and initial conditions have been provided by global model Global Forecast System (GFS) (Environmental Modeling Center, 2003) at 00 UTC of the day of each considered event. Boundary conditions instead have been provided to WRF model every three hours. The two events that affected the Po valley (July 2020 and September 2021) lasted some hours and took place in the afternoon, so their simulation is expected to be poorly affected by the model spin-up. The two events that interested Liguria (October 2019 and October 2021) instead, lasted almost 20 h, starting early in the morning (at about 5 UTC). However, it has been shown that high-resolution numerical weather prediction (NWP) models generally are able to produce dynamically consistent fine-scale structures and to produce the climatologically appropriate energy spectrum just in few hours of simulation. Structures and energy in the mesoscale are generated in a short time (hours), even though these structures are missing from the initial conditions (Skamarock, 2004). Furthermore, for these two events, the choice of a spin-up time of about 5 h is due by the use of the initial and boundary conditions provided by GFS 00 UTC run. This particular global model run has been selected for being one of the latest global model run available to simulate the particular heavy rain events, so to reduce at the most errors and biases coming from synoptic forecast (Mazzarella et al., 2021). So, also for the analysis of these events, we neglected spin-up effects.

Regarding the model setup, in the outer domain, the Betts-Miller-Janjic convection scheme (Betts and Miller, 1993) is used. Four km grid spacing falls into the so-called convective grey zone, where small-scale convective elements are partially resolved, but recent works have identified this convection scheme as one of the best performing also when it is exploited in 3 to 5 km resolution simulations (Avolio and Federico, 2018; Amirudin et al., 2022; Prat et al., 2021). In the inner domain convection is solved explicitely. To describe the subgrid-scale processes related to radiation physics, the Rapid Radiation Transfer Model (RRTM) (Mlawer et al., 1997) and the Dudhia (Skamarock et al., 2008) parameterization schemes have been chosen respectively for long-wave and short-wave radiation. Given the focus of the work on heavy precipitation, the sensitivity study involved parameterizations that are supposed to play a major role in describing evolution of precipitation driven by deep convection. To this purpose, having fixed the long-wave and short-wave radiation schemes over the two domains, as well as the cumulus scheme over the outermost domain, 30 CM, 8 PBL, 2 SL parameterization schemes, as well as 5 L-S models, chosen among the ones available in WRF model, Version 4.3.3, have been tested. Table 1 summarises the schemes exploited in the present study according to the code (second column) used by WRF model to identify each scheme. As control configuration, that is, as reference point of our sensitivity test, the configuration adopted for operational simulations at Centro Meteo Expert (*https : //www.meteo.expert/*), has been assumed. This WRF model configuration is routinely used for operational weather forecast in Italy, for media to all sectors were weather fields are important for daily operations such as energy, trading, transportation, logistic etc. Such a configuration is summarized in Table 2, and, in addition to the aforementioned parameterizations regarding short wave and long wave radiation, it includes Ferrier microphysics (Ferrier et al., 2002), YSU PBL scheme (Hu et al., 2013), Monin–Obukhov SL scheme (Grell et al., 1994)

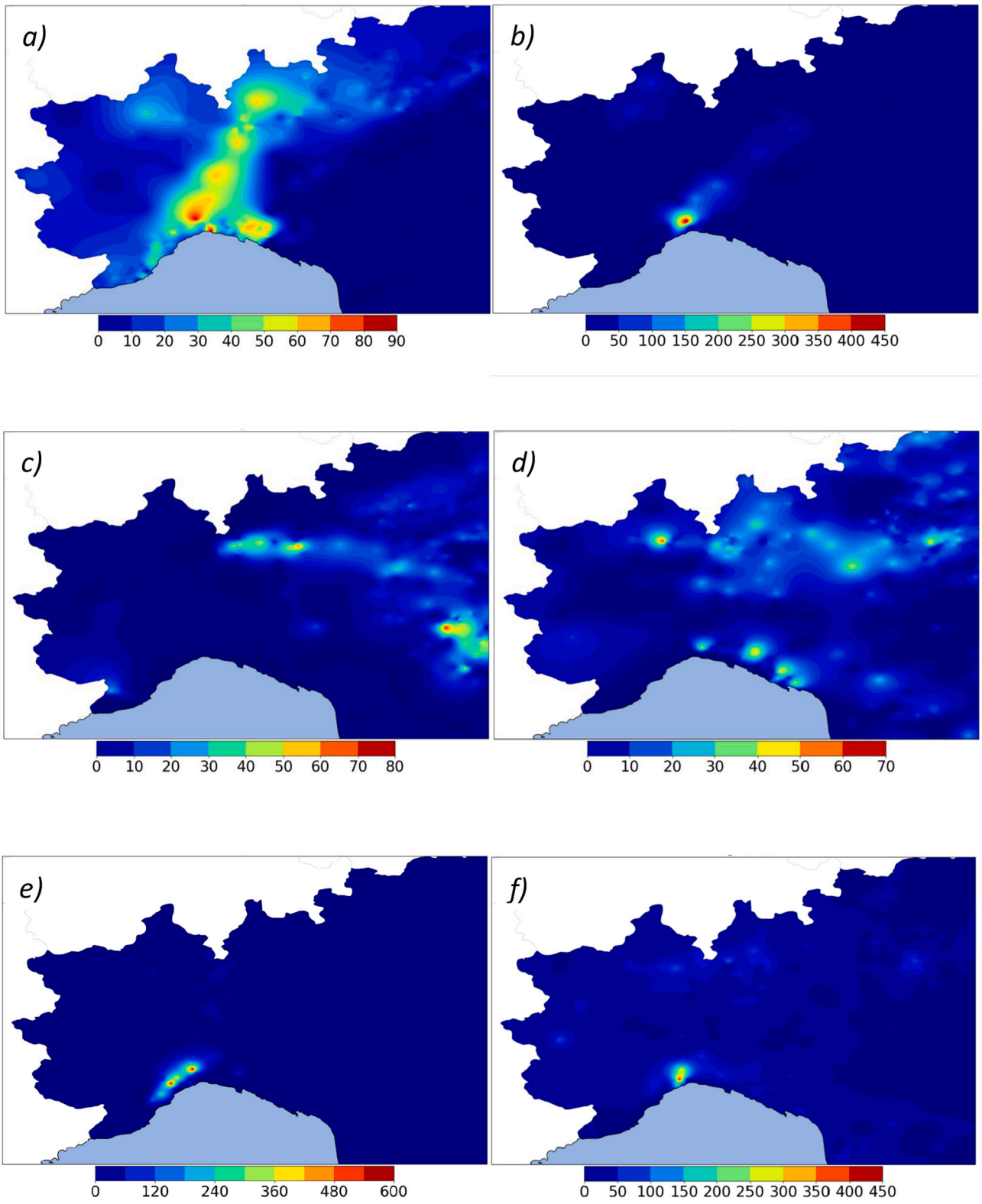

Fig. 2. Accumulated precipitation (in millimeters) observed over North-Western Italy for the events considered in this work: panel *a*), from 00 UTC to 12 UTC of 21 October 2019; panel *b*), from 12 UTC of 21 October 2019 to 00 UTC of 22 October 2019; panel *c*), from 12 UTC of 11 of July 2020 to 00 UTC of 12 of July 2020; panel *d*), from 12 UTC of 16 September 2021 to 00 UTC of 17 September 2021; panel *e*), from 00 UTC to 12 UTC of 4 October 2021 and, panel *f*), from 12 UTC of 4 October 2021 to 00 UTC of 5 October 2021.

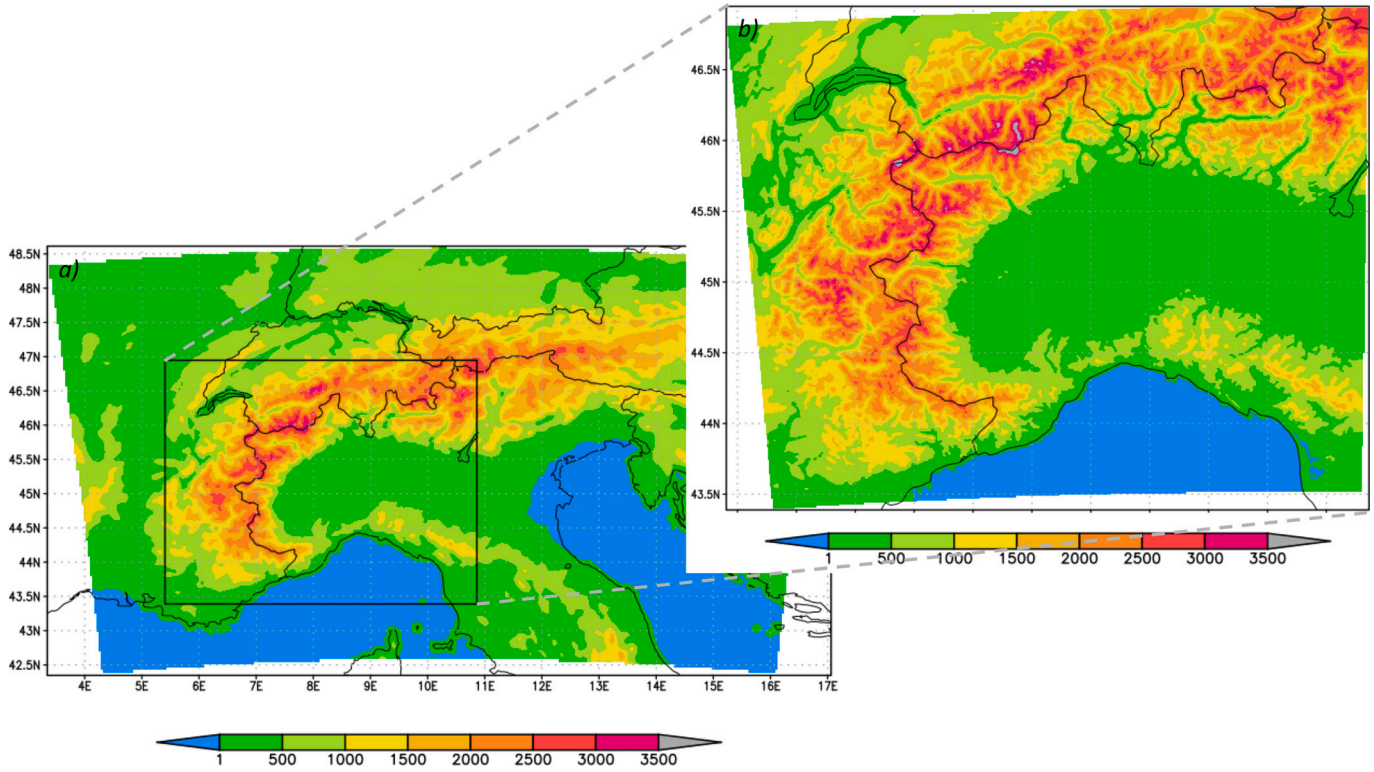

Fig. 3. Panel *a*): digital elevation model [m] of WRF simulation domains. Resolution of the domains varies from 4 km for the outermost domain to 1 km over the innermost domain. Panel *b*): a zoom of the higher resolution domain.

Table 1
Tested WRF parameterization schemes. First and third columns indicate the parametrized physical process, while second and fourth columns indicate the WRF parameterization code.

Physical process	*Scheme*	*Physical process*	*Scheme*
CM	1	CM	51
CM	2	CM	52
CM	3	CM	53
CM	4	CM	55
CM	5	CM	56
CM	6	CM	95
CM	7	CM	97
CM	8	PBL	1
CM	9	PBL	5
CM	10	PBL	6
CM	11	PBL	7
CM	13	PBL	11
CM	14	PBL	12
CM	16	PBL	16
CM	17	PBL	99
CM	18	SL	1
CM	19	SL	91
CM	21	L-S	1
CM	24	L-S	2
CM	26	L-S	3
CM	28	L-S	4
CM	50	L-S	5

and the Unified Noah L-S model (Chen and Dudhia, 2001; Campbell et al., 2019). To limit the number of possible parameterizations combinations, a cascade approach has been applied. Starting from the control configuration, a set of parameterization schemes has been tested one-at-a-time, in order to identify the best performing scheme to be used for the following parameterizations set test. The order of the parameterization schemes to test has been chosen on the basis of the expected role played by the schemes themselves on precipitation, i.e., in decreasing order with reference to the expected impact on precipitation

Table 2
WRF parameterization schemes adopted as control configuration.

Physical process	*Scheme*	Reference
Long-wave radiation	1	(Mlawer et al., 1997)
Short-wave radiation	1	(Skamarock et al., 2008)
Cloud microphysics	5	(Ferrier et al., 2002)
Planetary Boundary Layer	1	(Hu et al., 2013)
Surface Layer	91	(Grell et al., 1994)
Land-Surface model	1	(Chen and Dudhia, 2001; Campbell et al., 2019)

modeling. More specifically, starting from the control configuration, PBL, SL and L-S schemes have been kept fixed and 30 runs for each event have been performed, a run for each of the 30 CM schemes available in the WRF model. Once the best performing microphysical parameterization scheme has been identified, such scheme has been fixed to evaluate the performances of the PBL parameterization schemes, by keeping fixed the SL scheme and the L-S model. An analogous procedure is adopted to test the SL schemes, and finally the L-S models. Globally, 45 different configurations have been tested. Since not all PBL, SL and L-S parameterization schemes available in WRF model are compatible with the adopted control configuration, only a subset of these schemes entered in the sensitivity study.

Finally, observed precipitation fields, necessary to assess the simulations quality and shown in Fig. 2, have been obtained through Ordinary Kriging (Ly et al., 2011) interpolation of data coming from two sources: about 1,200 citizen-science meteorological stations spread across Northern Italy and courteously provided by Meteonetwork (*https : //www.meteonetwork.it/*), a non-profit organization devoted to promote and disseminate the knowledge of meteorological science (Giazzi et al., 2022); about 200 rain gauges provided by the regional rain gauge network of Liguria, OMIRL (Osservatorio Meteo Idrologico della Regione Liguria), managed by the Ligurian Regional Environmental

Protection Agency (ARPAL).

4. Analysis methodology

An objective quantification of the reliability of the results from high-resolution simulations is a very challenging problem, especially when studying convective phenomena resulting in severe precipitation extremely localized in space and time, as those analized in the present work. The first difficulty is the lack of sufficiently spatially detailed rain data in order to provide a realistic observed field able to describe the spatial variability of the fine-scale precipitation patterns that characterize these events. In our case, about 1,400 rain gauges cover an area of about 70,000 km^2 and, although not uniformly distributed, provide data sufficient to describe the main characteristics of spatial variability of the studied events. A second problem for the verification of high-resolution simulations emerges when using categorical indexes based on the definition of contingency tables, the so called 'double penalty' error (Lack et al., 2010; Zingerle and Nurmi, 2008). This kind of point-based verification is indeed very sensitive to a small displacement of precipitation patterns: even a relatively small spatio-temporal shift of features, which are correctly described in terms of intensity and size, might yield very poor categorical scores (Rossa et al., 2008). To overcome this issue, different new-generation spatial verification techniques have been developed. In particular, for our analysis, the Method for Object-Based Diagnostic Evaluation (MODE) (Davis et al., 2006; Davis et al., 2006) has been exploited. This method is based on the evaluation of the coupling degree between patterns (in our case precipitation areas above a certain threshold) identified both in the observed and simulated fields. This approach is particularly suitable to evaluate the model capability to reproduce structures associated to high-precipitation events produced by convective systems, which need high-resolution simulations to be correctly described. The coupling between observed and simulated features is calculated through the definition of an index that weighs different characteristics of the identified objects, such as spatial extension, displacement, intensity, orientation and so on. This method too, however, suffers from some drawbacks. Even if patterns of interest have been identified both in the simulated and observed fields, it remains quite challenging to asses which couples of simulated and observed objects refer to the same phenomenon and therefore have to be considered, and which couples comply to different convective systems so that they should be rejected. In the following paragraphs of this section, the methodology adopted to overcome these problems and to obtain the most objective evaluation of the performances of the simulations is presented step by step.

The first step concerned the choice of the threshold necessary to identify the objects associated to the phenomena under study. Since the present work is focused on the ability of the model to reproduce intense precipitation, high threshold values have been selected. The thresholds have been fixed as the 60 % of the precipitation maxima in the observed 12-h accumulated precipitation fields, obtained from interpolation of rain gauges observations. Namely we considered six twelve-hours-long time intervals as summarized in Table 3, where the observed maxima and the corresponding threshold used to identify precipitation patterns are reported. Once the thresholds have been fixed, the connected areas where the precipitation field is above the selected thresholds constitute the objects in the precipitation field and identify the precipitation patterns.

Such patterns have been identified both in forecast and observed fields and a coupling index, *CI*, for any forecasted and observed objects pair has been derived, by weighing different attributes through an algorithm (Davis et al., 2009):

$$CI_j = \frac{\sum_{i=1}^{M} w_i F_{i,j}}{\sum_{i=1}^{M} w_i} \tag{1}$$

where j refers to the j-th pair of objects considered, M is the total number of attributes considered and each attribute is identified with the index i. $F_{i,j}$ is the interest function that prescribes, on a scale from 0 to 1, how closely the i-th forecast attribute matches the observed one for the j-th couple of objects. $F_{i,j} = 1$ corresponds to a perfect matching. The coefficients w_i are the weights assigned to each attribute when computing a *CI* value for objects pairs.

Davis et al. (2009) added a further coefficient, p_i, which multiplies w_i. Such a coefficient is used when the confidence in one attribute is dependent on the value of another attribute. The more significant example is the observed wind direction provided by an anemometer, whose confidence is related to the wind intensity (when the wind intensity is too weak, the observed direction is poorly resolved). In our case however, we will consider attributes which are independent of each other, such as centroid distance, spatial extension, extension of the intersection area and precipitation intensity within the objects boundaries. Therefore, p_i will be assumed constant and equal to 1.

Even if the choice of the parameters reported in (1) is subjective and not universal, once these parameters have been fixed according to the specific focus of the research, this index provides a quite robust way to compare different simulations and to produce a hierarchy of best performing settings, helping to highlight even the smallest improvements associated to the different parameterizations.

The evaluation of the coupling between forecast and observed objects provides a good instrument to judge the capability of the model to reproduce observed patterns, but does not provide information about the tendency to under- or over-estimate precipitation. In other words, a simulation that produces an erroneously high number of precipitation structures, some of which perfectly stackable to the observed ones, will result in high values of *CI*, despite a global overestimation of the precipitation. In the same way, a simulation that underestimates precipitation, but that is able to reproduce a small subset of the observed structures only, will again result in good values of the presented index.

To overcome this problem and taking into account also the aptitude of the simulation to under- or over-estimate precipitation, the *CI* has been merged with two traditional point-wise indexes widely used in numerical models performances evaluation. In particular, Fals Alarm Rate (*FAR*) and Critical Success Index (*CSI*) (Wilks, 2006) have been used in this work: both indexes are based on punctual matching between forecasts and observations. After defining a precipitation threshold, it is possible to create a contingency table, like the one reported in Table 4, that summarizes all the possible combinations of forecast and observed precipitation above or below the given threshold (Wilks, 2006).

Table 3
Dates of the analyzed case studies (first column), observed precipitation maxima for twelve-hours-long time intervals (second column) and precipitation thresholds used to identify precipitation patterns both in the observed and forecast fields (third column).

Precipitation accumulation period	*Observed maxima [mm]*	*Threshold [mm]*
00 UTC 2019/10/21–12 UTC 2019/10/21	86.6	49.3
12 UTC 2019/10/21–00 UTC 2019/10/22	450.6	262.4
12 UTC 2020/7/11–00 UTC 2020/7/12	72.4	41.6
12 UTC 2021/16/9–00 UTC 2021/9/17	60.7	35.2
00 UTC 2021/20/4–12 UTC 2021/10/4	587.6	330.6
12 UTC 2021/10/4–00 UTC 2021/10/5	423.4	246.9

Table 4
2 × 2 contingency table in terms of counts of observed and forecasted precipitation for a selected threshold.

	Observed	Not observed
Forecasted	n_{11}	n_{10}
Not forecasted	n_{01}	n_{00}

FAR is defined as the ratio of false alarms, i.e., erroneous prediction of intense precipitation, over the total number of non observed events:

$$FAR = \frac{n_{10}}{n_{10} + n_{00}} \quad (2)$$

FAR ranges from 0 to 1, where 0 corresponds to a perfect forecast.

CSI, instead, represents the ratio of the number of times the event was correctly forecasted to occur over the number of times it was either forecasted or occurred:

$$CSI = \frac{n_{11}}{n_{11} + n_{10} + n_{01}} \quad (3)$$

CSI values are in the range from 0 to 1, and 1 corresponds to a perfect forecast. In our case, the comparison involved the whole observed and simulated fields, i.e. all grid points belonging to the simulated and observed fields entered in the calculation of the indexes in order to have an overall evaluation of the precipitation under- or over-estimation of the model. These two indexes have been therefore merged with *CI*, to compute a Global Index (*GI*) able to measure the capability of the simulations to create the observed phenomena structures and the global tendency of the simulations to over- or under-estimate precipitation. *GI* is defined as:

$$GI = (1 - FAR)*CI*CSI \quad (4)$$

GI = 1 corresponds to a perfect matching between forecast and observation.

5. Results and discussions

5.1. Cloud michophysics parameterization schemes sensitivity analysis

5.1.1. Object-oriented verification

As described in the previous section, the first step of the cascade sensitivity test involved varying 30 different CM parameterization schemes, keeping fixed other parameterizations as the reference configuration.

As this work is focused on extreme events characterized by intense precipitation over small areas, the most relevant attributes to be taken into account in the computation of the coupling degree between pairs of simulated and observed objects, according to the *CI* index defined in (1), have been centroid distance, spatial extension, extension of the intersection area and precipitation intensity within the objects boundaries. These attributes have been equally weighted, i.e, the relative weights w_i reported in (1) assumed the same value (namely 1) in order to give equal importance to the four considered attributes when calculating the *CI*. Fig. 4 summarizes, for each model setting, the number of forecast-observed pairs that stay in each *CI* interval reported on the vertical axis, normalized to the total number of objects pairs associated to each scheme. In the picture, different values of the *CI* index (vertical axis) are reported versus the different CM schemes analyzed. The colored boxes represent the number of forecast-observed pairs (normalized to the total number of forecast-observed pairs associated to each scheme) that present a *CI* index laying in the corresponding interval. The high number of objects pairs found in correspondence of low *CI* values (i.e. the high number of forecast and observed patterns that present completely different features) does not necessarily means bad performance of the model. In the calculation of the *CI* index, precipitation patterns that refer to spatially distinct events cannot be filtered out; every forecast-observed objects pair present in a certain simulation is considered, i.e., also structures that pertain to different convective cells are coupled. To clarify this remark, it is useful to think of an observation field in which two objects (O1 and O2), i.e. areas above a certain threshold, were individuated, and a corresponding forecast field in which the same features (F1 and F2) were exactly represented (in term of centroid distance, spatial extension, extension of the intersection area and

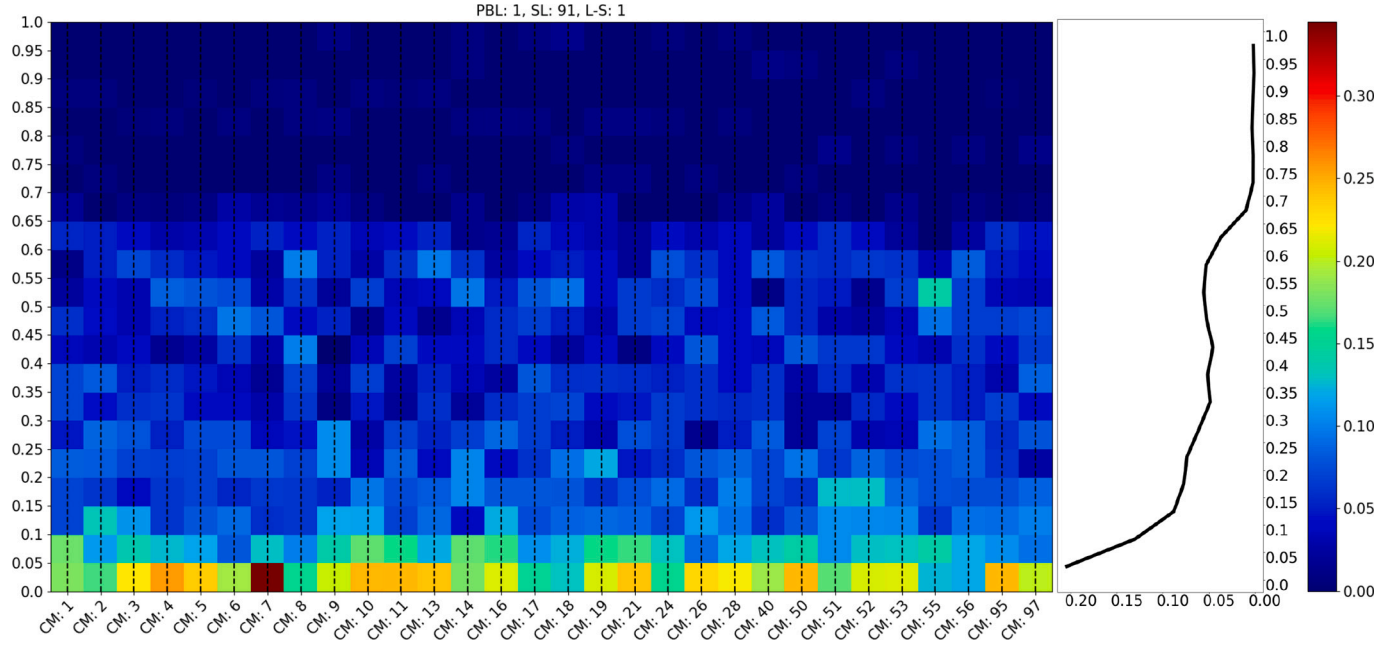

Fig. 4. Relative frequency [-] of forecast-observed objects pairs (values shown in the colorbar), for different intervals of *CI* values [-], left-hand vertical axis, for all CM parameterization schemes analyzed. Right hand panel represents the frequency average (horizontal axis [-]) for different intervals of *CI* values (vertical axis) regardless the CM parameterization applied.

precipitation intensity within the objects boundaries). When computing *CI*, the two well-coupled pairs (O1-F1 and O2-F2) will provide high contribution to *CI* values (namely 1 in an idealized perfect situation), whereas the other two pairs (associated to the spurious coupling of different convective cells O1-F2 and O2-F1) would contribute with two very low values to such an index (0 if the two pairs pertain to completely different precipitation patterns). This example explains the high number of objects pairs characterized by low values of *CI* present in Fig. 4 and furthermore rises the question about obtaining an objective method to neglect *CI* values referring to objects pairs that pertain to different convective cells. In other words, it is necessary to fix a *CI* threshold value under which it is reasonable to assume we are evaluating the coupling between objects that refer to different features. In Fig. 4 it is possible to observe how the number of pairs generally decreases for increasing *CI* values.

For values of *CI* in an approximate range between 0.45 and 0.6,

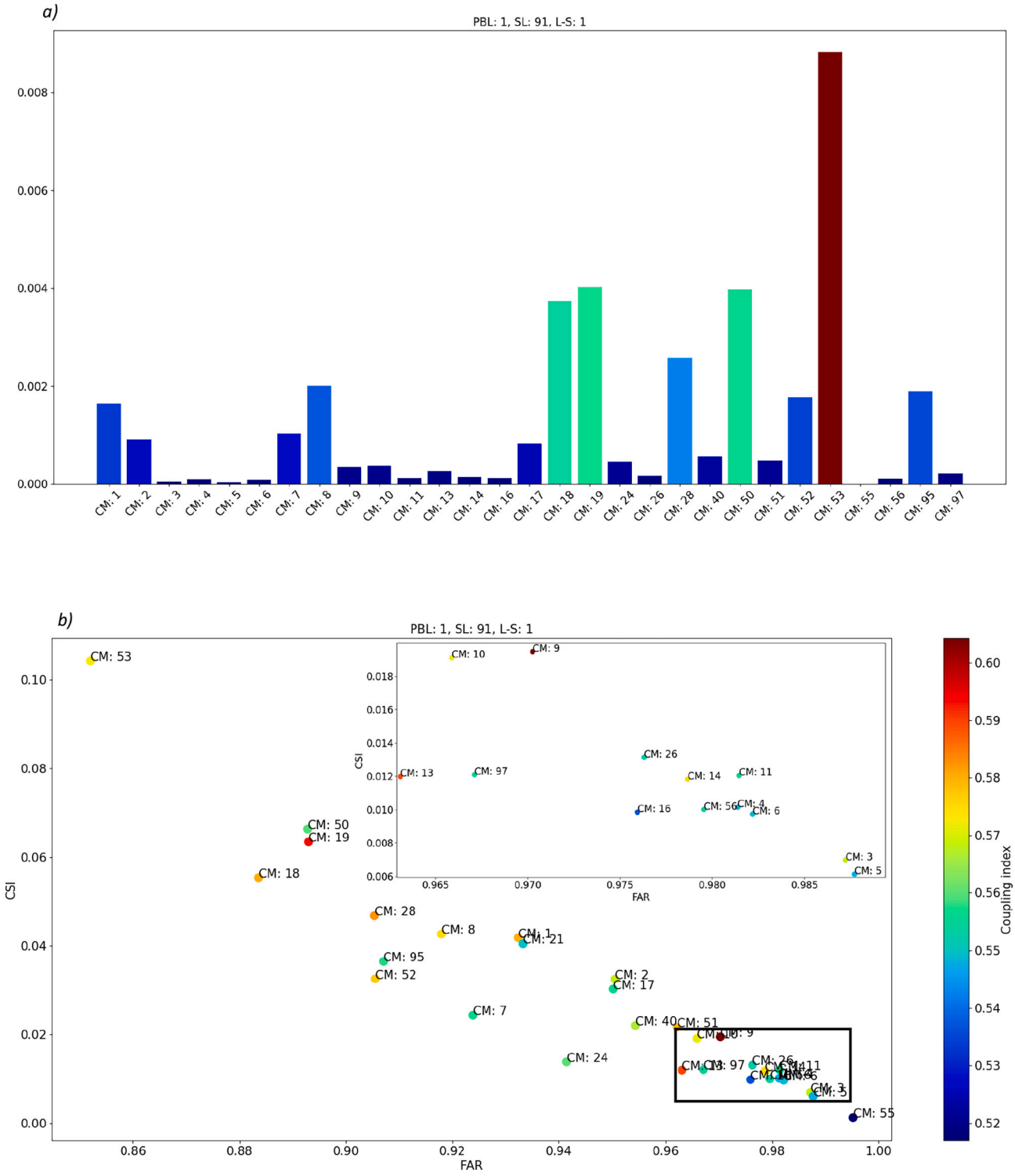

Fig. 5. Panel *a*) : *GI* [-] evaluated for all CM parameterization schemes tested. Panel *b*) : *CSI* [-], left-hand vertical axis, *FAR* [-], horizontal axis and *CI* [-], colorbar, values that entered in the calculation of *GI*, for each CM parameterization schemes tested.

however, it can be observed, on average, a slight increase in the corresponding population of forecast-observed objects pairs. This fact is well visible from the right-hand panel of Fig. 4, where the frequency of the forecast-observed pairs, that stay in each of the *CI* interval reported on the vertical axis, has been averaged regardless the CM parameterization applied. So, taking into account all objects produced by all simulations regardless the microphysical scheme applied, the distribution of their coupling degree with all observed precipitation patterns is described by the black line on the right of Fig. 4. The frequency peak observed for *CI* values between 0.45 and 0.6 indicates that starting from these *CI* values we are no more coupling objects that would not be considered, but we are matching structures that effectively pertain to the same physical phenomenon. For the following analysis, hence, $CI = 0.45$ has been chosen as the threshold to be taken into account in the calculation of *GI*.

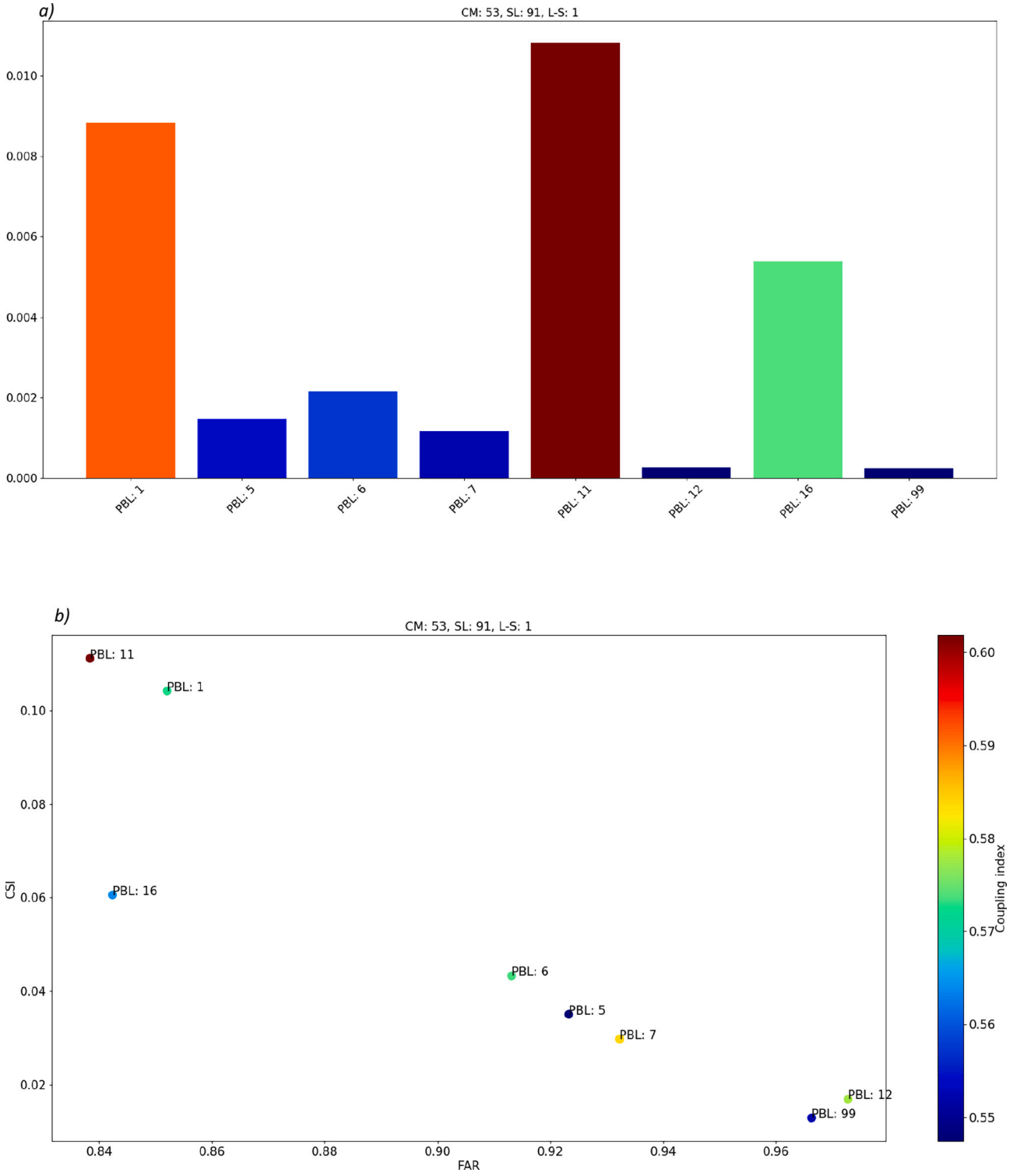

Fig. 6. Panel *a*) : *GI* [-] evaluated for all PBL parameterization schemes tested. Panel *b*) : *CSI* [-], left-hand vertical axis, *FAR* [-], horizontal axis and *CI* [-], colorbar, values that entered in the calculation of *GI*, for each PBL parameterization schemes tested.

5.1.2. Merged point-wise and object-oriented verification

In Fig. 5, panel *a*), *GI* is reported. The index has been evaluated for all tested CM schemes, and has been calculated from (4), where *FAR* and *CSI* have been averaged over all simulations corresponding to each model setting. *CI* instead enters in (4) as an average obtained considering, for each model setting, only objects pairs that present a *CI* value above the threshold individuated in the previous subsection. From this analysis, it clearly emerges that CM 53 outperforms the other schemes. The three different terms entering in the calculation of *GI* are individually plotted in Fig. 5, panel *b*), to explicitly show the weight of each parameter involved in the calculation of *GI*. CM 53 scheme provides the highest *CSI* value, the lowest *FAR* value among all CM schemes tested, as well as a quite high *CI* value, if compared with values provided by other CM schemes, finally resulting in the highest *GI*. This fact indicates a good compromise between over- or under-estimation of precipitation and quite good capability in reproducing observed structures. CM 53 scheme, that considerably outperforms all other schemes (Fig. 5, panel *a*)), is a double-moment scheme for cloud water, but it is the only scheme, among the ones available in the WRF model, to be triple-moment for ice phase (Milbrandt et al., 2021). The gap between CM 53 performance and those associated to all other schemes is quite surprisingly and suggests the fundamental role of this different way to treat ice particles within clouds. Although cloud ice is contemplated by all analized micophysical parameterizations, triple-moment ice schemes in principle result in a better representation of the ice particles size distribution evolution and may be important for some aspects of modeling secondary ice production, recognised as a fundamental cloud microphysical process (Cantrell and Heymsfield, 2005; Field et al., 2017), and its impacts on precipitation (Qu et al., 2022). Finally, a more accurate description of the evolution of cloud ice within the clouds through a triple-moment treatment can result in a more reliable simulation of the final precipitation. However, the development of triple-moment microphysical schemes is quite recent and these preliminary promising results suggest a more in-depth analysis of mechanisms underlying cloud ice interactions, also extending the set of case studies, in future works.

5.2. Planetary Boundary Layer schemes sensitivity analysis

Following the result obtained by the first step of the cascade sensitivity test, CM 53 scheme has been fixed and the 8 PBL schemes summarized in Table 1 have been tested. *GI* values for the different PBL schemes are reported in Fig. 6, panel *a*). In this case, PBL 11, corresponding to the Shin–Hong (SH) PBL parameterization scheme (Choi and Han, 2020), outperformed other schemes. SH PBL parameterization is a scale-aware scheme that considers the grid-size dependencies of subgrid-scale turbulent vertical transport and for which the local and nonlocal heat transports are separately calculated by considering grid-size dependencies; therefore it can be more efficient in triggering convection. Unfortunately, the lack of observations of fluxes along the vertical profile prevents from a more in-depth evaluation of PBL dynamics. In this case, the highest value of *GI*, associated to PBL 11 scheme, derives from individually best values of *FAR*, *CSI* and *CI* indexes (Fig. 6, panel *b*)). It is interesting to note that the range of values assumed by *GI* in analysing the PBL performances is similar to the range of values associated to the CM parameterization schemes analysis. Therefore, from this analysis, the PBL parameterization schemes appear to play a major role, at least as much as the CM schemes, in simulation of precipitation associated to intense convective events. This fact could be related to the different vertical diffusion schemes assumed by the different PBL parameterizations, resulting in a different low-level transport of moisture, heat and momentum through the PBL to higher levels and within cloud (Zampieri et al., 2005), that can in turn affect the triggering of the convection.

5.3. Surface Layer parameterization schemes sensitivity analysis

Results presented in the previous subsection, show the strong impact on simulations of the PBL schemes in complex terrain, and further justify the need to analyse the effect of the SL (namely the lowermost layer of the PBL) parameterization schemes on the simulation of deep convective systems. In fact, the atmospheric surface layer typically represents the lowest part of the PBL, up to about 50 m from the ground surface, where the mechanical generation of turbulence exceeds the buoyant generation or consumption (Businger et al., 1971; Srivastava et al., 2021), and once again can play a main role in triggering convection. In this case, since the SL and PBL schemes have often been designed to work with each other, only two SL schemes, SL 1 and SL 91, were compatible with the control configuration and PBL 11.

Fig. 7, panels *a*) and *b*), summarizes the results of the SL analysis. *GI* range (Fig. 7, panel *a*)), as well as the range of values assumed by *CSI*, *FAR* and *CI* (Fig. 7, panel *b*)) is smaller than those observed for CM and PBL schemes (Figs. 5 and 6) mainly because in this case only two SL have been analyzed. However, SL 91 parameterization, a scheme based on fifth generation Pennsylvania State University–National Center for Atmospheric Research Mesoscale Model (MM5) (Grell et al., 1994), has shown slight better performances and has been assumed for the following step of the sensitivity analysis.

5.4. Land-Surface models sensitivity analysis

The last part of the sensitivity study involved an evaluation of the impact that different L-S models have on precipitation simulated during the considered severe events. Five L-S models were compatible with WRF configuration individuated up to here and have been tested. These schemes are characterized by different degree of realism in the representation of soil physics, land cover type, soil water content, snow cover, drip, runoff or infiltration (García-García et al., 2022). As shown in many works, energy and water exchanges between the lower layer of the atmosphere and the ground surface can alter surface conditions, particularly during extreme weather events in summer (Seneviratne et al., 2006; Miralles et al., 2012; Hauser et al., 2016).

Fig. 7 shows again some variability both in *GI* (panel *c*)) and in individual *CSI*, *FAR* and *CI* indexes (panel *d*)) suggesting a high impact of L-S models on the simulation of the precipitation and allowing to individuate a best performing model. Strong influence of L-S model in convective initiation has been shown in a recent work (Henderson et al., 2022), where it has been demonstrated that different surface properties can lead to large discrepancies in the net surface radiative budget, particularly in the sensible and latent heating, that may significantly impact the timing and spatial evolution of convection and precipitation. L-S 1, the Unified Noah land-surface model adopted for control configuration (Chen and Dudhia, 2001; Campbell et al., 2019), shows the best *GI* and also the best individual *CSI*, *FAR* and *CI* indexes, concluding our sensitivity test.

Given the great importance that parameterization schemes have on the performances of NWP models, parameterizations have been the focus of numerous studies in recent years. However, comparisons among studies are complicated, in some cases there may be discrepancies between different findings, also because results depend on the studied areas and events, as well as on the method used to analyse simulations. For example, Merino et al. (2022) conducted a WRF sensitivity study focused on severe events in Ebro valley and found a predominant role of microphysical schemes with respect to PBL parameterization schemes, in partial discrepancy with results obtained in the present work. So, given the great importance of the topic, it might be useful to systematically compare case studies from many areas of the Mediterranean basin and the application of different methods of analysis, with the ultimate goal of improving robustness and value of the results.

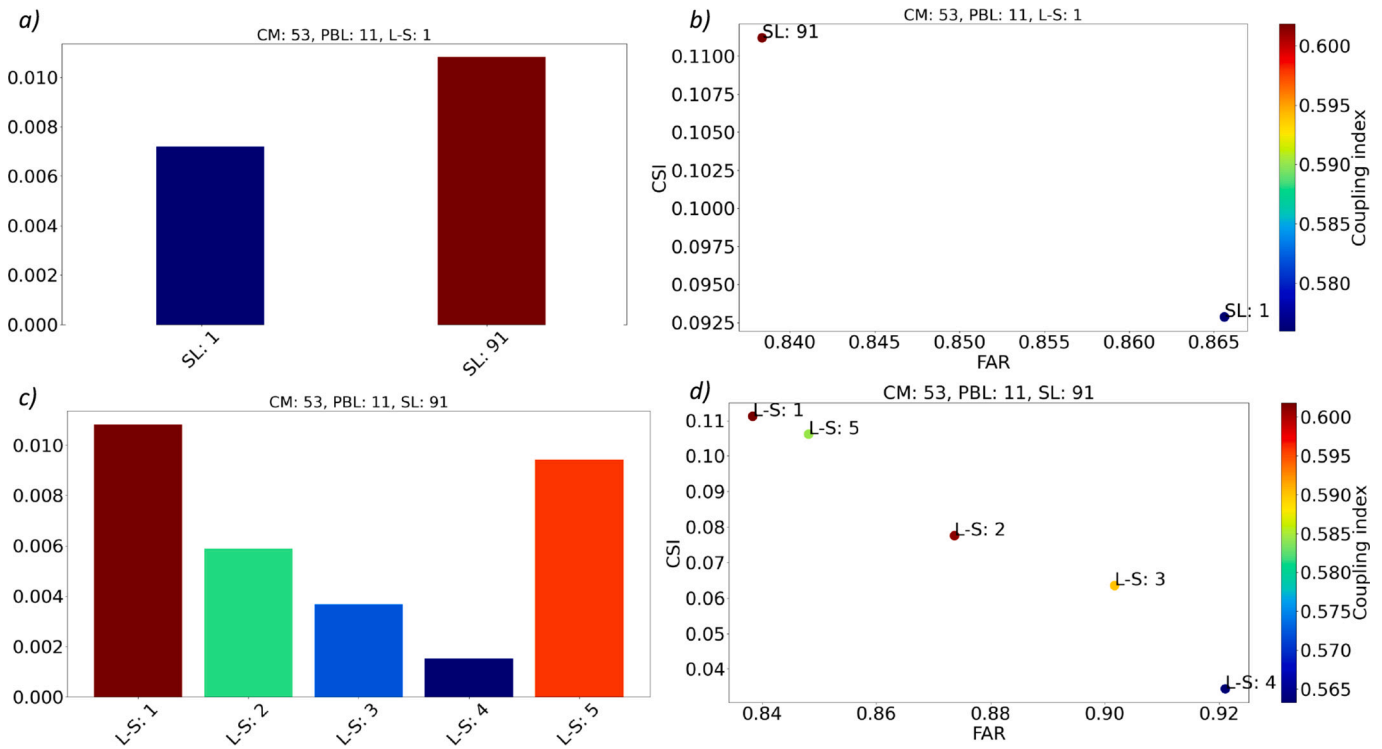

Fig. 7. Panel *a*) : *GI* [-] evaluated for all SL parameterization schemes tested. Panel *b*) : *CSI* [-], left-hand vertical axis, *FAR* [-], horizontal axis and *CI* [-], colorbar, values that entered in the calculation of *GI*, for each SL parameterization schemes tested. Panel *c*) : *GI* [-] evaluated for all L-S models tested. Panel *d*) : *CSI* [-], left-hand vertical axis, *FAR* [-], horizontal axis and *CI* [-], colorbar, values that entered in the calculation of *GI*, for each L-S models tested.

6. Conclusions and perspectives

In the present study, an expansive sensitivity test regarding different parameterization schemes available in WRF model, has been performed. Four significant precipitation events caused by the development of deep convective systems occurred in North-West Italy between 2019 and 2021 have been selected to test the performances of different model schemes. Globally, 45 high-resolution simulations (1 km grid step), corresponding to 45 different WRF settings, have been produced for each of the four events. The quality of the different configurations has been assessed through a so-called cascade sensitivity test during which, starting from a control configuration, 30 different CM, 8 PBL, 2 SL and 5 L-S parameterization schemes have been tested. The simulated precipitation fields have been compared with data from about 1,400 rain gauges spread across North-Western Italy, of which about 1,200 associated to citizen-science meteorological stations provided by Meteonetwork and about 200 from the regional rain gauge network of Liguria, OMIRL. Due to the well known 'double penalty' problem when evaluating high-resolution simulations through point-wise statistical indexes, an object-oriented verification based on MODE and obtained through the calculation of a coupling index (*CI*) between structures identified in observed and forecast fields, has been adopted. However, a stand-alone analysis based on the matching of observed-forecast precipitation patterns can be misleading when dealing with a high number of, observed and/or simulated, scattered structures. To overcome these problems, a Global Index, *GI*, obtained merging point-wise *FAR* and *CSI* indexes and the *CI* index deriving from object-oriented analysis, has been defined. *GI* provided an objective and reproducible instrument to emphasize also small differences in simulations allowing to obtain a hierarchy of best performing schemes.

Two are the most significant results of our cascade sensitivity test based on the evaluation of *GI*.

Firstly, the CM 53 significantly outperforms all other cloud microphysics parameterization schemes, presenting the highest *CSI* index and the lowest *FAR* index among microphysical schemes tested, as well as quite high value, with respect to the range of values assumed by other parameterizations, of *CI*. It is interesting to note that CM 53 is the unique cloud ice triple-moment scheme, highlighting the role of a triple-moment treatment of this hydrometeor in the description of the studied events.

Secondly, the range of values assumed by *GI* for different PBL schemes, as well as for different L-S models, is similar to the one observed for CM schemes, and therefore underlines the leading role of the PBL and L-S parameterizations in simulating precipitation associated to intense convective events. In fact, these schemes describe the subgrid-scale turbulent vertical transport in lower atmospheric layers, the energy and water exchanges between the lower layers of atmosphere and the ground surface, as well as the net surface radiative budget, all aspects that may strongly affect the triggering and the evolution of simulated precipitation for deep convective events. More difficult is to asses the role of the SL schemes being only two SL parameterizations compatible with the adopted control configuration.

This study is a promising work because the identified best performing WRF setting together with the defined analysis method provide the instruments for future evaluation of the impact on WRF performances of different data assimilation methods and input data. It is however worth mentioning that the presented cascade sensitivity test is driven by the need to reasonably limit the number of parameterization schemes combinations to study. The complex interaction between the different parametrized phenomena and the high impact that all different sets of tested schemes (CM, PBL, SL and L-S) have on model performances imply that this study can miss some specific combination of high-performance schemes. However, this work provides a quite robust analysis method that could be applied in future to an extended set of parameterizations.

CRediT authorship contribution statement

Francesco Ferrari: Conceptualization, Methodology, Software, Formal-analysis, Data-curation, Writing-original-draft. **Enrico Maggioni:** Conceptualization, Methodology, Data-curation, Writing-review-editing. **Alessandro Perotto:** Conceptualization, Methodology, Data-curation, Writing-review-editing. **Raffaele Salerno:** Conceptualization, Methodology, Writing-review-editing. **Mauro Giudici:** Conceptualization, Methodology, Writing-review-editing.

Declaration of Competing Interest

The authors declare that they have no known competing financial interests or personal relationships that could have appeared to influence the work reported in this paper.

Data availability

The data that has been used is confidential.

Acknowledgement

This work has been conducted within the project "ENDAS - Enhancement of data assimilation and data driven modeling to improve the meteorological predictions at different space and time scales", financed through the PON "Ricerca e Innovazione" 2014–2020, Action IV.6 "Research contracts on Green themes".

Mauro Giudici contributed to this research partially in the framework of the project "Geosciences for society: resources and their evolution" supported by the Italian Ministry of University and Research (MUR) through the funds 'Dipartimenti di Eccellenza 2023–2027'.

References

Amirudin, A.A., Salimun, E., Zuhairi, M., Tangang, F., Juneng, L., Mohd, M.S.F., Chung, J.X., 2022. The importance of cumulus parameterization and resolution in simulating rainfall over peninsular malaysia. Atmosphere 13.

Avolio, E., Federico, S., 2018. WRF simulations for a heavy rainfall event in southern Italy: verification and sensitivity tests. Atmos. Res. 209, 14–35. https://doi.org/10.1016/j.atmosres.2018.03.009.

Betts, A.K., Miller, M.J., 1993. The Betts-Miller Scheme. American Meteorological Society. pp. 107–121. doi:10.1007/978-1-935704-13-3.

Braun, S.A., Tao, W.K., 2000. Sensitivity of high-resolution simulations of hurricane Bob (1991) to planetary boundary layer parameterizations. Mon. Weather Rev. 128, 3941–3961. https://doi.org/10.1175/1520-0493(2000)129<3941:SOHRSO>2.0.CO;2.

Bryan, G.H., Morrison, H., 2012. Sensitivity of a simulated squall line to horizontal resolution and parameterization of microphysics. Mon. Weather Rev. 140, 202–225. https://doi.org/10.1175/MWR-D-11-00046.1.

Burlingame, B.M., Evans, C., Roebber, P.J., 2017. The influence of PBL parameterization on the practical predictability of convection initiation during the mesoscale predictability experiment (MPEX). Weath. Forecast. 32, 1161–1183. https://doi.org/10.1175/WAF-D-16-0174.1.

Businger, J.A., Wyngaard, J.C., Izumi, Y., Bradley, E.F., 1971. Flux-profile relationships in the atmospheric surface layer. J. Atmos. Sci. 28, 181–189. https://doi.org/10.1175/1520-0469(1971)028<0181:FPRITA>2.0.CO;2.

Buzzi, A., Davolio, S., Malguzzi, P., Drofa, O., Mastrangelo, D., 2014. Heavy rainfall episodes over Liguria of autumn 2011: numerical forecasting experiments. Nat. Hazards Earth Syst. Sci. 14, 1325–1340.

Campbell, P.C., Bash, J.O., Spero, T.L., 2019. Updates to the Noah land surface model in WRF-CMAQ to improve simulated meteorology, air quality, and deposition. J Adv Model Earth Syst 11, 231–256. https://doi.org/10.1029/2018MS001422.

Cantrell, W., Heymsfield, A., 2005. Production of ice in tropospheric clouds: a review. Bull. Am. Meteorol. Soc. 86, 795–808.

Casati, B., Wilson, L.J., Stephenson, D.B., Nurmi, P., Ghelli, A., Pocernich, M., Damrath, U., Ebert, E.E., Brown, B.G., Mason, S., 2008. Review forecast verification: current status and future directions. Meteorol. Appl. 15, 3–18.

Cassola, F., Ferrari, F., Mazzino, A., 2015. Numerical simulations of mediterranean heavy precipitation events with the WRF model: A verification exercise using different approaches. Atmos. Res. 164–165, 3–18.

Cassola, F., Ferrari, F., Mazzino, A., Miglietta, M.M., 2016. The role of the sea on the flash floods events over Liguria (northwestern Italy). Geophys. Res. Lett. 43, 3534–3542.

Chen, F., Dudhia, J., 2001. Coupling an advanced land-surface/hydrology model with the Penn state/NCAR MM5 modeling system. Part I: model description and implementation. Mon. Weather Rev. 12, 569–585.

Chen, X., Zhao, K., Xue, M., 2014. Spatial and temporal characteristics of warm seasonconvection over Pearl River Delta region, China, based on 3 years of operational radar data. J. Geophys. Res.: Atmos. 119, 12447–12465.

Choi, H.J., Han, J.Y., 2020. Effect of scale-aware nonlocal planetary boundary layer scheme on lake-effect precipitation at gray-zone resolutions. Mon. Weather Rev. 148, 2761–2776. https://doi.org/10.1175/MWR-D-19-0282.1.

Clark, A.J., Coniglio, M.C., Coffer, B.E., Thompson, G., Xue, M., Kong, F., 2015. Sensitivity of 24-h forecast dryline position and structure to boundary layer parameterizations in convection-allowing WRF model simulations. Weath. Forecast. 30, 613–638. https://doi.org/10.1175/WAF-D-14-00078.1.

Cohen, A.E., Cavallo, S.M., Coniglio, M.C., Brooks, H.E., 2015. A review of planetary boundary layer parameterization schemes and their sensitivity in simulating southeastern U.S. cold season severe weather environments. Weath. Forecast. 30, 591–612. https://doi.org/10.1175/WAF-D-14-00105.1.

Comellas Prat, A., Federico, S., Torcasio, R.C., Fierro, A.O., Dietrich, S., 2021. Lightning data assimilation in the WRF-ARW model for short-term rainfall forecasts of three severe storm cases in Italy. Atmos. Res. 247, 105246 https://doi.org/10.1016/j.atmosres.2020.105246.

Coniglio, M., Correia, J., Marsh, P., Kong, F., 2013. Verification of convection-allowing WRF model forecasts of the planetary boundary layer using sounding observations. Weath. Forecast. 28, 842–862.

Davis, A.C., Brown, B., Bullock, R., 2006. Object-based verification of precipitation forecasts. Part I: methodology and application to mesoscale rain areas. Mon. Wea. Rev. 134, 1772–1784.

Davis, A.C., Brown, B., Bullock, R., 2006. Object-based verification of precipitation forecasts. Part II: application to convective rain system. Mon. Wea. Rev. 134, 1785–1795.

Davis, A.C., Brown, B., Bullock, R., Halley-Gotway, J., 2009. The method for object based diagnosic evaluation (MODE) applied to numerical forecasts from the 2005 NSSL/SPC spring program. Wea. Forecast. 24, 1252–1267.

Dong, M., Ji, C., Chen, F., Wang, Y., 2019. Numerical study of boundary layer structure and rainfall after landfall of typhoon Fitow (2013): Sensitivity to planetary boundary layer parameterization. Adv. Atmos. Sci. 36, 1861–9533. https://doi.org/10.1007/s00376-018-7281-9.

Douluri, D.L., Chakraborty, A., 2021. Assessment of WRF-ARW model parameterization schemes for extreme heavy precipitation events associated with atmospheric rivers over west coast of India. Atmos. Res. 249, 105330 https://doi.org/10.1016/j.atmosres.2020.105330.

Efstathiou, G.A., Zoumakis, N.M., Melas, D., Lolis, C.J., Kassomenos, P., 2013. Sensitivity of WRF to boundary layer parameterizations in simulating a heavy rainfall event using different microphysical schemes. Effect on large-scale processes. Atmos. Res. 125–143.

Environmental Modeling Center, 2003. The GFS Atmospheric Model. NCEP Office Note 442. National Oceanic and Atmospheric Administration.

Ferrari, F., Cassola, F., Tuju, P., Mazzino, A., 2021. RANS and LES face to face for forecasting extreme precipitation events in the Liguria region (northwestern Italy). Atmos. Res. 259, 105654 https://doi.org/10.1016/j.atmosres.2021.105654.

Ferrier, B., Jin, Y., Lin, Y., Black, T., Rogers, E., Dimego, G., 2002. Implementation of a new grid-scale cloud and precipitation scheme in the NCEP Eta model. In: 15th Conf. on Numerical Weather Prediction, 280–283.

Field, P.R., Lawson, R.P., Brown, P.R.A., Lloyd, G., Westbrook, C., Moisseev, D., Miltenberger, A., Nenes, A., Blyth, A., Choularton, T., Connolly, P., Buehl, J., Crosier, J., Cui, Z., Dearden, C., DeMott, P., Flossmann, A., Heymsfield, A., Huang, Y., Kalesse, H., Kanji, Z.A., Korolev, A., Kirchgaessner, A., Lasher-Trapp, S., Leisner, T., McFarquhar, G., Phillips, V., Stith, J., Sullivan, S., 2017. Secondary ice production: Current state of the science and recommendations for the future. Meteorol. Monogr. 58, 7.1–7.20.

Fiori, E., Commellas, A., Molini, L., Rebora, N., Siccardi, F., Gochis, D.J., Tanelli, S., Parodi, A., 2014. Analysis and hindcast simulation of an extreme rainfall event in the Mediterranean area: the Genoa 2011 case. Atmos. Res. 138, 13–29.

Gao, Z., Zhu, J., Guo, Y., Luo, N., Fu, Y., Wang, T., 2021. Impact of land surface processes on a record-breaking rainfall event on may 06–07, 2017, in Guangzhou, China. J. Geophys. Res.: Atmos. 126, e2020JD032997. doi:10.1029/2020JD032997.

García-García, A., Cuesta-Valero, F.J., Beltrami, H., González-Rouco, J.F., García-Bustamante, E., 2022. WRF vol 3.9 sensitivity to land surface model and horizontal resolution changes over North America. Geoscient. Model Develop. 15, 413–428. https://doi.org/10.5194/gmd-15-413-2022.

Giazzi, M., Peressutti, G., Cerri, L., Fumi, M., Riva, I.F., Chini, A., Ferrari, G., Cioni, G., Franch, G., Tartari, G., Galbiati, F., Condemi, V., Ceppi, A., 2022. Meteonetwork: An open crowdsourced weather data system. Atmosphere 13. https://doi.org/10.3390/atmos13060928.

Gilleland, E., Ahijevych, D., Brown, B.G., Casati, B., Ebert, E.E., 2009. Intercomparison of spatial forecast verification methods. Wea. Forecast. 24, 1416–1430.

Grell, G., Dudhia, J., D.R.Stauffer, 1994. A description of the fifth-generation Penn State/NCAR Mesoscale Model (MM5). Technical Report. doi:10.5065/D60Z716B.

Han, J.Y., Baik, J.J., 2008. A theoretical and numerical study of urban heat island–induced circulation and convection. J. Atmos. Sci. 65, 1859–1877. https://doi.org/10.1175/2007JAS2326.1.

Hauser, M., Orth, R., Seneviratne, S.I., 2016. Role of soil moisture versus recent climate change for the 2010 heat wave in western Russia. Geophys. Res. Lett. 43, 2819–2826. https://doi.org/10.1002/2016GL068036.

Henderson, D.S., Otkin, J.A., Mecikalski, J.R., 2022. Examining the role of the land surface on convection using high-resolution model forecasts over the southeastern United States. J. Geophys. Res.: Atmos. 127 https://doi.org/10.1029/2022JD036563.

Holtslag, A.A.M., Svensson, G., Baas, P., Basu, S., Beare, B., Beljaars, A.C.M., Bosveld, F. C., Cuxart, J., Lindvall, J., Steeneveld, G.J., Tjernström, M., Wiel, B.J.H.V.D., 2013. Stable atmospheric boundary layers and diurnal cycles: Challenges for weather and climate models. Bull. Am. Meteorol. Soc. 94, 1691–1706. https://doi.org/10.1175/BAMS-D-11-00187.1.

Hong, S.Y., Noh, Y., Dudhia, J., 2006. A new vertical diffusion package with an explicit treatment of entrainment processes. Mon. Weather Rev. 134, 2318–2341. https://doi.org/10.1175/MWR3199.1.

Hu, X.M., Klein, P.M., Xue, M., 2013. Evaluation of the updated YSU planetary boundary layer scheme within WRF for wind resource and air quality assessments. J. Geophys. Res.: Atmos. 118, 10490–10505. https://doi.org/10.1002/jgrd.50823.

Hu, X.M., Nielsen-Gammon, J.W., Zhang, F., 2010. Evaluation of three planetary boundary layer schemes in the WRF model. J. Appl. Meteorol. Climatol. 49, 1831–1844. https://doi.org/10.1175/2010JAMC2432.1.

Lack, S.A., Limpert, G.L., Fox, N.I., 2010. An object-oriented multiscale verification scheme. Wea. Forecast. 25, 79–92.

Li, X., Pu, Z., 2008. Sensitivity of numerical simulation of early rapid intensification of hurricane Emily (2005) to cloud microphysical and planetary boundary layer parameterizations. Mon. Weather Rev. 136, 4819–4838. https://doi.org/10.1175/2008MWR2366.1.

Liu, J., Zhang, F., Pu, Z., 2017. Numerical simulation of the rapid intensification of hurricane Katrina (2005): Sensitivity to boundary layer parameterization schemes. Adv. Atmos. Sci. 34 https://doi.org/10.1007/s00376-016-6209-5.

Lorenz, R., Argüeso, D., Donat, M.G., Pitman, A.J., van den Hurk, B., Berg, A., Lawrence, D.M., Chéruy, F., Ducharne, A., Hagemann, S., Meier, A., Milly, P.C.D., Seneviratne, S.I., 2016. Influence of land-atmosphere feedbacks on temperature and precipitation extremes in the GLACE-CMIP5 ensemble. J. Geophys. Res.: Atmos. 121, 607–623. https://doi.org/10.1002/2015JD024053.

Ly, S., Charles, C., Degré, A., 2011. Geostatistical interpolation of daily rainfall at catchment scale: the use of several variogram models in the ourthe and ambleve catchments, belgium. Hydrol. Earth Syst. Sci. 15, 2259–2274. https://doi.org/10.5194/hess-15-2259-2011.

Maggioni, E., Manzoni, T., Perotto, A., Spada, F., Borroni, A., Giurato, M., Giudici, M., Ferrari, F., Zardi, D., Salerno, R., 2023. WRF data assimilation of weather stations and lightning data for a convective event in Northern Italy. Submitted to Bulletin of Atmospheric Science and Technology.

Mazzarella, V., Ferretti, R., Picciotti, E., Marzano, F.S., 2021. Investigating 3d and 4d variational rapid-update-cycling assimilation of weather radar reflectivity for a heavy rain event in central Italy. Natural Hazards and Earth System Sciences 21, 2849–2865. https://doi.org/10.5194/nhess-21-2849-2021.

Merino, A., García-Ortega, E., Navarro, A., Sánchez, J.L., Tapiador, F.J., 2022. WRF hourly evaluation for extreme precipitation events. Atmos. Res. 274, 106215 https://doi.org/10.1016/j.atmosres.2022.106215.

Miglietta, M.M., Davolio, S., 2022. Dynamical forcings in heavy precipitation events over Italy: lessons from the HyMeX SOP1 campaign. Hydrol. Earth Syst. Sci. 26, 627–646. https://doi.org/10.5194/hess-26-627-2022.

Milbrandt, J.A., Morrison, H., II, D.T.D., Paukert, M., 2021. A triple-moment representation of ice in the predicted particle properties (P3) microphysics scheme. Journal of the Atmospheric Sciences 78, 439 – 458. doi:10.1175/JAS-D-20-0084.1.

Miralles, D.G., van den Berg, M.J., Teuling, A.J., de Jeu, R.A.M., 2012. Soil moisture-temperature coupling: A multiscale observational analysis. Geophys. Res. Lett. 39 https://doi.org/10.1029/2012GL053703.

Mlawer, E.J., Taubman, S.J., Brown, P.D., Iacono, M.J., Clough, S.A., 1997. Radiative transfer for inhomogeneous atmosphere: RRTM, a validated correlated k-model for the long-wave. J. Geophys. Res. 102, 663–682.

Morrison, H., Milbrandt, J., 2011. Comparison of two-moment bulk microphysics schemes in idealized supercell thunderstorm simulations. Mon. Wea. Rev. 139, 1103–1130.

Niyogi, D., Pyle, P., Lei, M., Arya, S.P., Kishtawal, C.M., Shepherd, M., Chen, F., Wolfe, B., 2011. Urban modification of thunderstorms: An observational storm climatology and model case study for the Indianapolis urban region. J. Appl. Meteorol. Climatol. 50, 1129–1144. https://doi.org/10.1175/2010JAMC1836.1.

Pielke Sr, R.A., 2013. Mesoscale Meteorological Modeling. 3rd ed., Academic Press.

Pleim, J.E., 2007. A combined local and nonlocal closure model for the atmospheric boundary layer. part I: Model description and testing. J. Appl. Meteorol. Climatol. 46, 1383–1395. https://doi.org/10.1175/jam2539.1.

Pleim, J.E., 2007. A combined local and nonlocal closure model for the atmospheric boundary layer. part II: Application and evaluation in a mesoscale meteorological model. J. Appl. Meteorol. Climatol. 46, 1396–1409. https://doi.org/10.1175/JAM2534.1.

Qu, Z., Korolev, A., Milbrandt, J.A., Heckman, I., Huang, Y., McFarquhar, G.M., Morrison, H., Wolde, M., Nguyen, C., 2022. The impacts of secondary ice production on microphysics and dynamics in tropical convection. EGUsphere 2022, 1–40. https://doi.org/10.5194/egusphere-2022-235.

Rajeevan, M., Kesarkar, A., Thampi, S.B., Rao, T.N., Radhakrishna, B., Rajasekhar, M., 2010. Sensitivity of WRF cloud microphysics to simulations of a severe thunderstorm event over Southeast India. Ann. Geophys. 28, 603–619.

Rebora, N., Molini, L., Casella, E., Commellas, A., Fiori, E., Pignone, F., Siccardi, F., Silvestro, F., Tanelli, S., Parodi, A., 2013. Extreme rainfall in the Mediterranean: what can we learn from observations? J. of Hydrometeorology 14, 906–922.

Roebber, P.J., Schultz, D.M., Colle, B.A., Stensrud, D.J., 2004. Toward improved prediction: High-resolution and ensemble modeling systems in operations. Weather and Forecasting 19, 936–949. https://doi.org/10.1175/1520-0434(2004)019<0936:TIPHAE>2.0.CO;2.

Rossa, A., Nurmi, P., Ebert, E., 2008. Precipitation: advances in measurement, estimation and prediction. Springer Berlin Heidelberg. chapter 16. pp. 417–450.

Seneviratne, S.I., D, L., Litschi, M., Schar, C., 2006. Land–atmosphere coupling and climate change in Europe. Nature 443, 205–209.

Shin, H.H., Hong, S.Y., 2011. Intercomparison of planetary boundary-layer parametrizations in the WRF model for a single day from CASES-99. Bound.-Layer Meteorol. 139, 261–281.

Skamarock, W.C., 2004. Evaluating mesoscale NWP models using kinetic energy spectra. Mon. Weather Rev. 132, 3019–3032. https://doi.org/10.1175/MWR2830.1.

Skamarock, W.C., Klemp, J.B., Dudhia, J., Gil, D.O., Barker, D.M., Duda, M.G., Huang, X. Y., Wang, W., Powers, J.G., 2008. A Description of the Advanced Research WRF Version 3. Technical Report. National Center for Atmospheric Research.

Srinivas, C., Yesubabu, V., Hari Prasad, D., Hari Prasad, K., Greeshma, M., Baskaran, R., Venkatraman, B., 2018. Simulation of an extreme heavy rainfall event over Chennai, India using WRF: Sensitivity to grid resolution and boundary layer physics. Atmos. Res. 210, 66–82. https://doi.org/10.1016/j.atmosres.2018.04.014.

Srivastava, P., Sharan, M., Kumar, M., 2021. A note on surface layer parameterizations in the weather research and forecast model. Dyn. Atmos. Oceans 96, 101259. https://doi.org/10.1016/j.dynatmoce.2021.101259.

Wang, R., Zhu, Y., Qiao, F., Liang, X.Z., Zhang, H., Ding, Y., 2021. High-resolution simulation of an extreme heavy rainfall event in Shanghai using the weather research and forecasting model: Sensitivity to planetary boundary layer parameterization. Advances in Atmospheric Sciences 38.

Wilks, D.S., 2006. Statistical methods in the atmospheric sciences, volume 91. Elsevier.

Xu, W., Zipser, E.J., Chen, Y.L., Liu, C., Liou, Y.C., Lee, W.C., Jou, B.J.D., 2012. An orography-associated extreme rainfall event during TiMREX: Initiation, storm evolution, and maintenance. Mon. Weather Rev. 140, 2555–2574. https://doi.org/10.1175/MWR-D-11-00208.1.

Zampieri, M., Malguzzi, P., Buzzi, A., 2005. Sensitivity of quantitative precipitation forecasts to boundary layer parameterization: a flash flood case study in the Western Mediterranean. Nat. Hazards Earth Syst. Sci. 5, 603–612.

Zingerle, C., Nurmi, P., 2008. Monitoring and verifying cloud forecasts originating from operational numerical models. Meteorol. Appl. 15, 325–330. https://doi.org/10.1002/met.73.